Study of direct-drive, deuterium–tritium gas-filled plastic capsule implosions using nuclear diagnostics at OMEGA

C. K. Li, F. H. Séguin, D. G. Hicks,[a] J. A. Frenje, K. M. Green, S. Kurebayashi, and R. D. Petrasso[b]
Plasma Science and Fusion Center, Massachusetts Institute of Technology, Cambridge, Massachusetts 02139

D. D. Meyerhofer,[c] J. M. Soures, V. Yu. Glebov, R. L. Keck, P. B. Radha, S. Roberts, W. Seka, S. Skupsky, and C. Stoeckl
Laboratory for Laser Energetics, University of Rochester, Rochester, New York 16423

T. C. Sangster
Lawrence Livermore National Laboratory, Livermore, California 94550

(Received 24 April 2001; accepted 31 July 2001)

Implosions of direct-drive, deuterium–tritium (DT) gas-filled plastic capsules are studied using nuclear diagnostics at the OMEGA laser facility [T. R. Boehly *et al.*, Opt. Commun. **133**, 495 (1997)]. In addition to traditional neutron measurements, comprehensive sets of spectra of deuterons, tritons, and protons elastically scattered from the fuel and shell by primary DT neutrons (''knock-on'' particles) are, for the first time, obtained and used for characterizing target performance. It is shown with these measurements that, for 15-atm DT capsules with 20-μm CH shells, improvement of target performance is achieved when on-target irradiation nonuniformity is reduced. Specifically, with a two-dimensional (2D) single-color-cycle, 1-THz-bandwidth smoothing by spectral dispersion (SSD), plus polarization smoothing (PS), a primary neutron yield of $\sim 1 \times 10^{13}$, a fuel areal density of $\sim$15 mg/cm^2, and a shell areal density of $\sim$60 mg/cm^2 are obtained; these are, respectively, $\sim$80%, $\sim$60%, and $\sim$35% higher than those achieved using 0.35-THz, 3-color-cycle, 2D SSD without PS. (In determining fuel areal density we assume the fuel to have equal numbers of D and T.) With full beam smoothing, implosions with moderate radial convergence ($\sim$10–15) are shown to have ρR performance close to one-dimensional-code predictions, but a ratio of measured-to-predicted primary neutron yield of $\sim$0.3. Other capsules that are predicted to have much higher radial convergence (3.8-atm DT gas with 20-μm CH shell) are shown to have $\rho R_{\text{fuel}} \sim 3$ mg/cm^2, falling short of prediction by about a factor of 5. The corresponding convergence ratios are similar to the values for 15-atm capsules. This indicates, not surprisingly, that the effects of mix are more deleterious for high-convergence implosions. A brief comparison of these moderate- and high-convergence implosions to those of similar deuterium–deuterium (D_2) gas-filled capsules shows comparable hydrodynamic performance. © *2001 American Institute of Physics.* [DOI: 10.1063/1.1405016]

I. INTRODUCTION

High-gain inertial confinement fusion (ICF) requires symmetric compression of a spherical capsule to a state of high density and temperature,[1–4] and current research is aimed at finding ways of achieving this goal. In this paper we utilize a range of traditional and new nuclear diagnostics to study the compression performance of deuterium–tritium (DT) gas-filled target capsules imploded by direct laser drive at the 60-beam OMEGA laser system.[5] We demonstrate the sensitivity of implosion performance to uniformity of laser power deposition, and investigate the effects of fuel-gas pressure, by measuring fuel and shell areal density (ρR) and shell electron temperatures (T_e). The study of these parameters is accomplished through the first comprehensive set of spectral measurements of deuterons, tritons, and protons (''knock-ons'') elastically scattered from the fuel and shell by 14.1-MeV DT fusion neutrons.

To achieve ICF ignition, a DT-filled target needs sufficient compression to form two different regions: a small mass with low density but high temperature in the center (the ''hot spot,'' with $T_i \sim 10$ keV) and a large mass of high density, low temperature fuel surrounding this hot spot. The 3.5-MeV DT alphas generated in the central hot spot (with $\rho R \sim 0.3$ g/cm^2) will be stopped in the fuel, propagating a thermonuclear burn. Two approaches to achieving this objective involve indirect- or direct-drive implosion of target capsules. For the indirect-drive approach, where laser beams irradiate the inner wall of a high-Z radiation case (hohlraum), laser energy is first converted to soft x rays which subsequently compress the capsule. The direct-drive approach utilizes laser beams directly irradiating and compressing the target. The National Ignition Facility (NIF), which will have both

[a] Present address: Lawrence Livermore National Laboratory.
[b] Also senior visiting scientist at Laboratory for Laser Energetics, University of Rochester.
[c] Also at Departments of Mechanical Engineering and Physics, and Astronomy, University of Rochester.

indirect- and direct-drive capabilities and is under construction at Lawrence Livermore National Laboratory, is designed to achieve this ignition objective. Experiments on OMEGA are currently investigating many aspects of the implosion physics relevant to the future NIF experiments with scaled experimental conditions. For example, the OMEGA cryogenic program will study energy-scaled implosions based on NIF ignition target designs.[6]

OMEGA is a Nd-doped glass laser facility, with an ability to deliver 60 beams of frequency-tripled UV light (351 nm) with up to 30 kJ in 1–3 ns with a variety of pulse shapes.[5] Early direct-drive experiments at OMEGA have achieved high temperatures ($T_i \sim 15$ keV) and high fusion yields (for example, DT neutron yield $\sim 10^{14}$ and DD neutron yield $\sim 10^{12}$).[7] In particular, a series of implosions of room-temperature capsules with gas fill (0 to 30 atm of either D_2 or D ^{3}He) and plastic shells (CH, 10 to 35 μm thick) has recently been conducted with a variety of laser pulse shapes, of irradiation uniformities, etc.[8–12] These implosions generate typical fuel areal densities (ρR_{fuel}) of ~5–15 mg/cm^2 and shell areal densities (ρR_{shell}) ~50–75 mg/cm^2. They provide insight into implosion physics of direct-drive ICF and planned OMEGA cryogenic-target implosions.

This paper presents the results of implosions of room-temperature capsules with DT gas fill and CH shells. The capsules nominally have 20-μm shell thickness and either 15-atm or 3-atm fill pressure. These capsules have diameters (~920–960 μm) and total masses similar to those of OMEGA cryogenic targets, and are expected to have comparable stability properties under similar experimental conditions.[6,8] OMEGA cryogenic capsules consist of three parts: a central part with low-pressure (triple-point vapor pressure) D_2 or DT gas (0.2 atm at ~19 K); a main fuel layer (~90 μm of D_2 or DT ice); and a 1–3 μm CH overcoat. The CH shell of a room-temperature target simulates the fuel part (DT ice) of a cryogenic target, and the fill gas simulates the hot-spot-forming central DT gas in a cryogenic target.[6] The hydrodynamics are expected to differ in detail, due, in part to the differences in the equation of state, ablation rate, and implosion velocity. Nevertheless, many aspects of high-energy-density physics and the target performances of cryogenic targets can be studied with these surrogate targets under current experimental conditions, including the effects of irradiation uniformity. The experiments also provide useful data for the development of advanced diagnostics (such as high-resolution charged-particle spectroscopy[13]) and for benchmarking computer simulations.[14]

A primary emphasis in this study is the dependence of capsule performance on laser irradiation uniformity, and Sec. II provides motivation by describing the importance of irradiation uniformity to the physics of capsule implosion performance. Section III describes the experiments utilizing DT-filled capsules with CH shells and different laser smoothing techniques. Section IV discusses the measurement of knock-on spectra and the relationships between these measurements and the characteristics of imploded capsules. Section V discusses the performance of imploded core and shell under different conditions, showing that 15-atm DT capsules with appropriate laser smoothing achieved a moderate convergence ratio (Cr ~10–15); ρR_{fuel} and ρR_{shell} were determined to be ~15 mg/cm^2 and ~60 mg/cm^2, respectively. We also studied implosions of capsules with 3.8-atm DT fill, which were predicted to have high-convergence-ratios (Cr ~30). Although we obtained a slightly lower ρR_{shell} ~55 mg/cm^2, core areal density falls short of the predictions by about a factor of 5 (~3 mg/cm^2). Furthermore, the effects of the time-dependent capsule charging and particle acceleration are, for the first time, experimentally proved to be unimportant for the circumstance of the experiment, since the bang time occurs several hundreds of ps after the laser is off. Section VI summarizes the major results.

II. LASER DRIVE CHARACTERISTICS AND CAPSULE PERFORMANCE

Successful direct-drive implosions require maintaining shell integrity during the acceleration phase by control of the Rayleigh–Taylor (RT) instability, because direct-dive targets are susceptible to this instability during both their acceleration and deceleration phases.[6,8] The instability is seeded by laser illumination nonuniformity, target imperfections (roughness on the outer ablative surface and/or the inner shell–fuel interface), and beam-to-beam power imbalance.[8] During the acceleration phase, this instability occurs at the ablation surface and propagates to the fuel–shell interface, adding roughness to the inner shell; in the worst case, this could lead to shell break-up. During the deceleration phase, the distortions at the fuel–shell interface grow and result in the mixing of fuel and shell materials, degrading the target performance.

For the shots studied here, two approaches were used for controlling instabilities and improving target performance. The first was a choice of laser-pulse shape. A high-shock-strength (high adiabat), 1-ns square laser pulse was used for maximizing the ablation rate and reducing the RT growth. Though a gradually rising pulse (low adiabat) produces, in principle, a larger target compression than a sharply rising pulse, due to lower fuel and shell isentropes,[1,2] a low-shock-strength pulse generates a lower ablation rate and smaller in-flight shell thickness, leading to more instability for direct-drive implosions. This has been demonstrated in earlier experiments, where better target performance was obtained with a 1-ns square pulse than with other pulse types for room-temperature targets.[9,10] Implosion of room-temperature capsules with 20-μm-CH shells using 1-ns square pulses results in stability properties that are similar to those of shaped-pulse-implosions of cryogenic targets (for example, the OMEGA $\alpha = 3$ design[8]).

The second approach is improved laser irradiation uniformity. In discussing deviations from illumination uniformity, we distinguish two sources. Beam-to-beam energy imbalance causes low-order mode perturbations (mode number $l < 10$), while nonuniformities within individual beams generates higher-order perturbations ($l > 10$). To achieve a level of 1% or less for on-target irradiation nonuniformity, different beam energies must be matched to within an rms deviation of <5%.[6,8] In the series of implosions studied here, an energy balance within 3–25% rms was achieved. However,

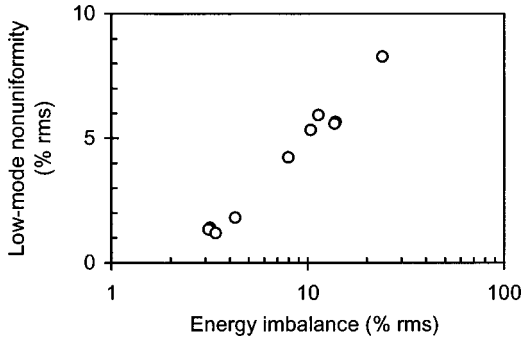

FIG. 1. The low-mode rms irradiation nonuniformity plotted as a function of the beam energy imbalance for different shots in this series of experiments. Better energy balance results in better low-mode rms irradiation uniformity. In this plot, the energy imbalance is an experimentally measured number which is based on the rms average of the energy of all 60 beams. This energy is measured with the HED system as described in LLE Rev. **63**, p. 110 (1995). The estimated precision of this measurement is ±1%. The energy measurements are input to a calculation that uses a generic (measured) DPP beam distribution and an assumed absorption profile to calculate the overlapped energy distribution on target. This overlapped intensity distribution is analyzed and the rms nonuniformity over spherical harmonic modes 1 to 10 is summed and used as the *y* coordinate in this plot. The most important error in this calculation is probably the assumption of equal beam profiles. We know from x-ray measurements of the beams on target that the DPP distributions do vary but we cannot give a precise estimate of the effect of this on the rms intensity distribution at this time.

after taking into account the effect of the laser-beam overlap on the target surface, as shown in Fig. 1, low-mode rms uniformity was between 1% and 9%, with an average $\leqslant 5\%$.

Single-beam uniformity is improved by two-dimensional smoothing by spectral dispersion (2D–SSD) combined with other smoothing techniques such as distributed phase plates (DPPs), and distributed polarization smoothing (PS) using birefringent wedges.[6,8] The two smoothing conditions used in this study are 0.35-THz-bandwidth, 3-color-cycle 2D–SSD and 1.0-THz-bandwidth, single-color-cycle 2D–SSD with PS. Theoretical simulations and recent experiments have demonstrated that PS results in improvement of irradiation uniformity by a factor of $\sim\sqrt{2}$ for higher-order perturbations ($l>10$). The combination of PS with high bandwidth 2D–SSD is expected to result in on-target nonuniformity $<1\%$ after 300 ps.[6,8,15]

III. EXPERIMENTS

The OMEGA experiments reported here used 60 beams of frequency-tripled (351 nm) UV light to directly drive the targets. Targets were room-temperature capsules with DT gas enclosed in a CH shell. The actual DT gas pressure was either 11–15 atm, for moderate-convergence capsules, or 3.8 atm, for high-convergence capsules; all nominally had equal-molar amounts of deuterium and tritium. The CH shell thickness was 19–20 μm, and the capsule diameters were 920–960 μm. The laser energy ranged from 20 to 23 kJ, with a typical intensity of $\sim 1\times 10^{15}\,\mathrm{W/cm^2}$, and the laser-beam spot size on target was ~1 mm. The laser pulse was 1-ns square, with rise and decay times of ~150 ps. Good pulse-shape repeatability was obtained, and the beam-to-beam laser energy balance was typically ~5% rms. Two laser configurations were used. In the first, individual beams were smoothed using 3-color-cycle 2D–SSD with a bandwidth of 0.35 THz. In the second, beams were smoothed by single-color-cycle 2D–SSD, with a wider bandwidth of 1.0 THz, and polarization smoothing (PS) using birefringent wedges.

The primary DT neutron yields were measured using Cu activation.[16] For this series of experiments, primary DT neutron yields were 10^{12}–10^{13}, with an estimated measurement error of ~10%. Ion temperatures, T_i, were measured using time-of-flight neutron Doppler widths (NTOF).[17–19] Typical values were 3.5–5 keV, with a measurement error of ~0.5 keV. Fusion burn history was obtained with the neutron temporal detector (NTD),[20] and the typical fusion burn durations here were 140–190 ps with bang times occurring at several hundred ps after the end of the laser pulse.

To obtain the areal densities for compressed fuel and shell (a fundamental measure of the implosion dynamics and quality), and to address other issues (such as the measurement of shell T_e, electrostatic potential due to capsule charging, etc.), spectra of emerging charged particles were measured with two magnet-based charged-particle spectrometers (CPS-1 and CPS-2)[21–24] and several "wedge-range-filter" (WRF) spectrometers.[12,13,21,22] The charged particles [knock-on deuterons (KOd), tritons (KOt), and protons (KOp)] are elastically scattered from the fuel and shell by 14.1 MeV DT neutrons.[25,26] For DT-capsule implosions on OMEGA, this is currently the only technique for studying fuel and shell areal densities. Other possible methods include neutron activation,[27] measurements of secondary[28,29] and tertiary products (neutrons and protons[29–31]), but these methods are not currently practical due to certain technical limitations. For example, a time-of-fight type, single-hit neutron detector array (MEDUSA[32,33]) has been routinely used to determine ρR_{fuel} of D_2 targets, but this technique cannot be applied to DT implosions because the detector array is completely saturated by the large primary neutron flux.

The two magnet-based charged-particle spectrometers CPS-1 and CPS-2 are nearly identical, and each utilizes a 7.6-kG permanent magnet[23,24] constructed of a neodymium–iron–boron alloy with a steel yoke. Incoming particles are collimated by a slit whose width can be varied between 1 and 10 mm (for acceptance of 10^{-6} to 10^{-5} of the total yield), as appropriate for expected flux levels. The magnet separates particles into different trajectories according to the ratio of momentum to charge. Pieces of CR-39 are used as particle detectors, and are positioned throughout the dispersed beam normal to the particle flux. Both the energy and the species of the particle generating a track in CR-39 can be determined through the combined knowledge of its trajectory (determined by its position on the CR-39) and the track diameter. Particles with the same gyro-radius, such as 8-MeV tritons and 12-MeV deuterons, are easily distinguished since their very different stopping powers generate measurably different track sizes in the CR-39 (the larger the stopping power, the larger the track). This configuration allows coverage over the proton energy range from 0.1 MeV to 40 MeV. The energy calibration uncertainty varies with particle energy, being about 30 keV at 2 MeV and about 100 keV at 15 MeV. The two spectrometers are 101° apart, thereby enabling studies of implosion symmetry to be undertaken. CPS-2 (CPS-1) is

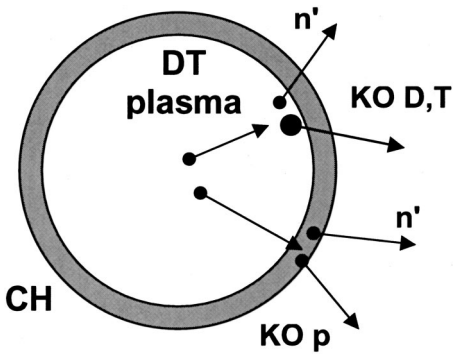

FIG. 2. A schematic of the knock-on processes in an imploded capsule. The central fuel part typically has an initial radius between 440–460 μm and a DT gas fill between 3–15 atm. The initial shell layer is constructed of CH with a thickness between 19–20 μm. Primary 14.1-MeV DT neutrons, generated in the fuel, elastically scatter deuterons and tritons out of the fuel and protons out of the shell. Consequently, information from the compressed core is carried out by these knock-on deuterons and tritons, and information from the compressed shell is carried out by knock-on protons. The energy downshifts of knock-on D and T spectra also contain information about the shell.

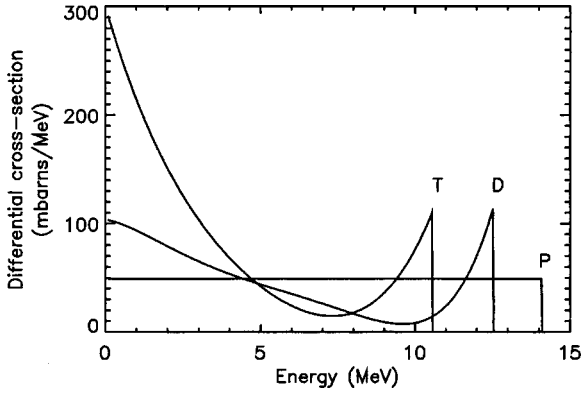

FIG. 3. Differential cross sections for elastic scattering of 14.1-MeV neutrons on deuterons, tritons, and protons, where the energy is the scattered ion energy. When these collisions are head-on, the characteristic endpoint (maximum) energy for T (D) [p] is 10.6 MeV (12.5 MeV) [14.1 MeV]. The high-energy peak for knock-on deuterons (tritons) contains about 15.7% (13.5%) of the total cross section, which corresponds to an energy region of 9.6–12.5 MeV (7.3–10.6 MeV). [For deuterons and tritons, the integral under the high-energy peak gives an effective cross-section that is used in Eq. (5). For knock-on protons, the cross section is flat from 0–14.1 MeV, and an integral over a 1-MeV interval gives an effective cross section that is used in Fig. 4.]

placed inside (outside) the 165-cm-radius OMEGA chamber at 100 cm (235 cm) from the target.

The WRF spectrometers, which are described in detail elsewhere,[12,13] provide proton spectra by analysis of the distributions of proton-track diameters in a piece of CR-39 that is covered during exposure by an aluminum ranging filter with continuously varying thickness. The current energy calibration is accurate to about 0.15 MeV at 15 MeV. They are simple and compact, allowing them to be used at multiple positions during a shot for symmetry studies and allowing them to be placed close to the target for good statistics when proton yields are low (down to about 5×10^5).

For comparison with measurements made during these experiments, the implosions were modeled with the one-dimensional hydrodynamic calculation code LILAC.[34] Several important physical models are utilized in the calculation, such as the tabulated equation of state (SESAME), flux-limited electron transport (with a flux limiter of $f=0.06$), local thermodynamic equilibrium (LTE), opacities for multi-group radiation transport, and inverse-bremsstrahlung-absorption energy deposition through a ray-trace algorithm in the under-dense plasma. No effect of fuel–shell mix is included.

IV. KNOCK-ON PARTICLES AND THEIR SPECTRA

Knock-on particles are generated in a two-step process. A 14.1-MeV neutron is first generated from a DT fusion reaction. These neutrons usually escape the capsule without interacting. However, a small fraction of them (of order ~0.1%) elastically scatter off either fuel D or T, or CH-shell p, as described in Eqs. (1)–(4) and depicted schematically in Fig. 2. Information about the compressed fuel is carried out by these knock-on D and T; information about the compressed shell is carried out by knock-on p and is also contained in the energy downshifts of knock-on D and T spectra:

$$\mathrm{D}+\mathrm{T}\rightarrow\alpha(3.5\,\mathrm{MeV})+n(14.1\,\mathrm{MeV}), \tag{1}$$

$$n(14.1\,\mathrm{MeV})+\mathrm{T}\rightarrow n'+\mathrm{T}(\leqslant 10.6\,\mathrm{MeV}), \tag{2}$$

$$n(14.1\,\mathrm{MeV})+\mathrm{D}\rightarrow n'+\mathrm{D}(\leqslant 12.5\,\mathrm{MeV}), \tag{3}$$

$$n(14.1\,\mathrm{MeV})+p\rightarrow n'+p(\leqslant 14.1\,\mathrm{MeV}). \tag{4}$$

Figure 3 illustrates the differential cross sections of knock-on processes. When the collisions are head-on, the characteristic endpoint energy for T(D)[p] is 10.6 MeV (12.5 MeV) [14.1 MeV]. The well-defined, high-energy peak for a knock-on deuteron (triton) spectrum represents about 15.7% (13.5%) of the total cross section, and corresponds to an energy region of 9.6–12.5 MeV (7.3–10.6 MeV). For a model-independent determination of ρR_{fuel}, the knock-on diagnostic usually only utilizes these high-energy peaks. For knock-on protons, the cross section is virtually flat from 0–14.1 MeV because the neutron and proton masses are nearly identical. However, because of a possible time-dependent distortion occurring in the low-energy region, only the flat region is utilized here. Two important parameters for this diagnostic are the number of knock-on particles and the downshifts of the knock-on spectra. The knock-on numbers provide information about the ρR of the layer (core or shell) in which they are produced, and the energy loss of these particles provides additional information about the ρR traversed.

For a hot-spot model of the compressed fuel (where all primary neutrons are produced in an infinitesimal, high temperature region at the center of a uniform density DT plasma), ρR_{fuel} is related to the knock-on yield by the equation[25,26]

$$\rho R_{\mathrm{fuel}}=\frac{(2\gamma+3)m_p}{(\gamma\sigma_d^{\mathrm{eff}}+\sigma_t^{\mathrm{eff}})}\,\frac{Y_{\mathrm{KO}d}+Y_{\mathrm{KO}t}}{Y_n}, \tag{5}$$

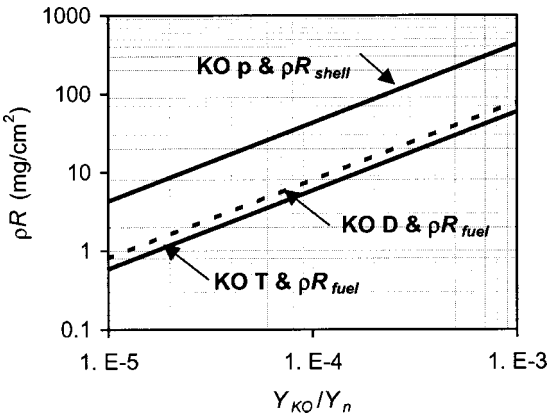

FIG. 4. Areal density vs the ratio of knock-on particle yield to primary neutron yield. For knock-on D and T, a hot-spot model is assumed and the yields under the high-energy peaks are used (as described in the caption of Fig. 3). For knock-on protons, a hot-spot model is assumed and the yield per MeV in the flat region is used.

where Y_n is the measured primary neutron yield, $Y_{\mathrm{KO}d}$ and $Y_{\mathrm{KO}t}$ are deuteron and triton knock-on yields under the high-energy peak of their spectra (see Fig. 3); $\sigma_t^{\mathrm{eff}}(\sigma_d^{\mathrm{eff}})$ is the effective cross section of knock-on triton (deuteron) as defined in Fig. 3; m_p is the proton mass; and $\gamma = n_d/n_t$. Similarly, the yield of knock-on protons, which are exclusively generated in the CH shell, can be shown to be related to ρR_{shell} by the equation

$$\rho R_{\mathrm{shell}} = \frac{(\gamma+12)m_p}{\gamma\sigma_p^{\mathrm{eff}}}\frac{Y_{\mathrm{KO}p}}{Y_n}, \tag{6}$$

where $Y_{\mathrm{KO}p}$ is the measured knock-on p yield in a 1-MeV range (see Fig. 3); σ_p^{eff} is an effective cross section for knock-on protons; and $\gamma = n_{\mathrm{H}}/n_{\mathrm{C}}$. Under some circumstances, it is useful to modify Eq. (5) for use with the ''uniform'' model, in which primary neutrons are generated throughout the volume containing deuterons and tritons, by multiplying the right-hand side by a factor of 1.33. Figure 4 displays inferred values of ρR as a function of the measured ratios of knock-on yield to primary neutron yield. The model-independent use of Eq. (5) breaks down when the total areal density exceeds about 100 mg/cm^2, because the knock-on spectra become sufficiently distorted by slowing-down effects that the measurements can become ambiguous; an accurate determination of ρR_{fuel} will then have to rely on model-dependent simulations.

The potential importance of knock-on particle measurements was realized some years ago, and measurements with limited spectral resolution and with a small number of knock-on particles (around 30) were subsequently obtained.[25,26] Those measurements relied on range-filter data in the form of ''coincident'' (front-side and back-side) tracks generated in a CR-39 nuclear track detector or in nuclear emulsions. This early work relied on detailed assumptions about the spectra of knock-on particles, which were estimated in indirect ways from other diagnostic data (for example, from the downshifted D ^{3}He protons).[25] In contrast, charged-particle spectroscopy, as described here, measures the whole spectrum directly for each particle. With hundreds

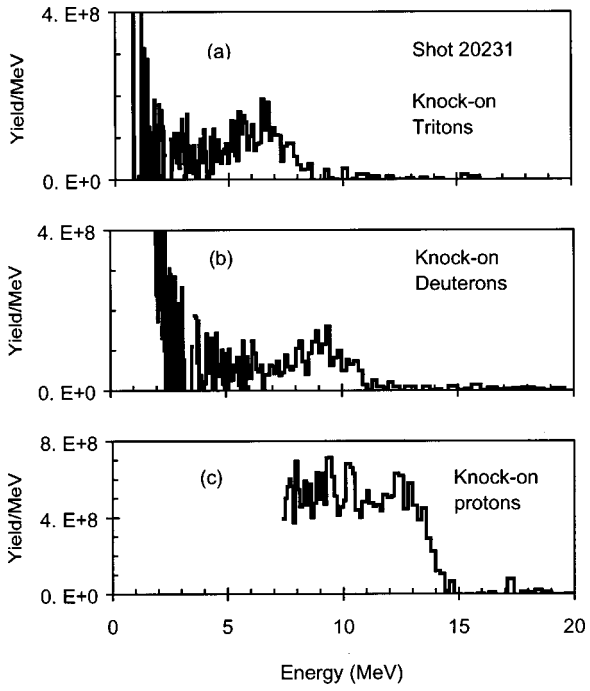

FIG. 5. Knock-on spectra measured by CPS-2 for shot 20231. The capsule was filled with 12.3 atm of DT gas and had a 19.1-μm CH shell. The laser energy is 22.1 kJ, and the primary neutron yields is 7.1×10^{12}. The 2D–SSD bandwidth is 0.35 THz, and no PS is applied. (a) The knock-on T spectrum, with a yield of about 5.7×10^8 tritons under the high-energy peak (between 3–10 MeV). The whole spectrum is downshifted by ~4 MeV (determined by the energy at which the yield/MeV reaches half of its peak value on the high-energy end of the spectrum). (b) The knock-on D spectrum, with a yield of about 4.8×10^8 deuterons under the high-energy peak (between 3.5–12 MeV). An energy loss of about ~3 MeV is measured. (c) The knock-on p spectrum with a yield/MeV of about 5.7×10^8 MeV protons in the flat region between 8–12 MeV. The endpoint of this spectrum is about 14 MeV, reflecting the fact that particles scattered from the outer part of the shell have no energy loss.

to thousands of knock-on particles being simultaneously detected from an individual implosion, comprehensive and high-resolution knock-on spectra are readily obtained.

Figure 5 shows sample spectra obtained by CPS-2 for shot 20231. For this shot, the capsule was filled with 12.3 atm of DT gas and had a 19.1-μm-thick CH shell. The laser energy was 22.1 kJ, and the primary neutron yield was $7.1(\pm0.7)\times10^{12}$. The 2D–SSD bandwidth was 0.35 THz, and no polarization smoothing (PS) was applied. The beam-to-beam energy balance was 13% rms, and the on-target, low-mode rms uniformity was 6% due to beam overlap on the target surface. An ion temperature of $T_i \cong 4.0$ (±0.5) keV was obtained. The fusion burn occurred at 1800(±50) ps and lasted for 180(±25) ps. Figure 5(a) provides the knock-on T spectrum with a yield of about 5.7×10^8 tritons under the high-energy peak (between 3–10 MeV). The whole spectrum is downshifted by ~4 MeV (as described in the figure caption). Figure 5(b) shows the knock-on D spectrum with a yield of about 4.8×10^8 deuterons under the high-energy peak (between 3.5–12 MeV). An energy loss of about ~3 MeV, relative to the birth spectrum, is measured. Figure 5(c) displays the knock-on p spectrum, with a yield of about 5.7×10^8 MeV protons in the flat region between 8–12 MeV. The endpoint of this spectrum is about 14 MeV, due to

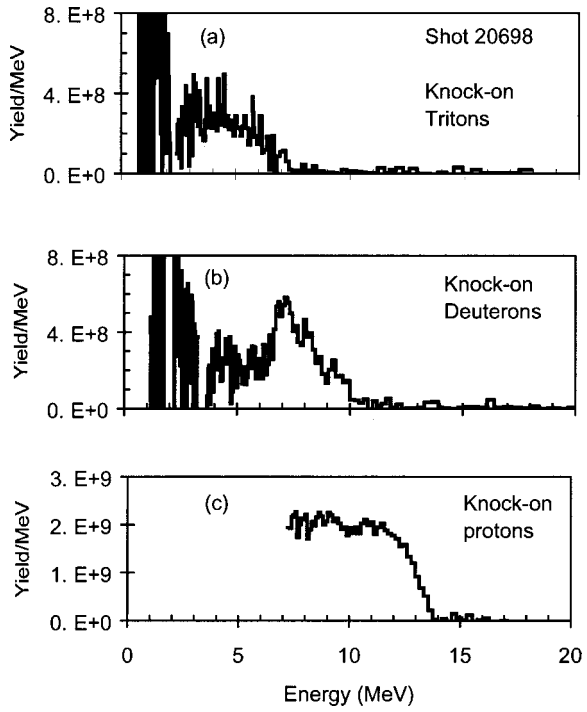

FIG. 6. Knock-on spectra for shot 20698, measured by CPS-2. The capsule is filled with 15 atm of DT gas and has a 20-μm CH shell. For this shot, the laser energy is 23.8 kJ, and the primary neutron yield is 1.4×10^{13}. The 2D–SSD bandwidth is 1.0 THz, and polarization smoothing (PS) is applied. (a) The knock-on T spectrum, with a yield of about 1.2×10^{9} tritons under the high-energy peak (between 2.5–10 MeV). The whole spectrum is downshifted by 4.8 MeV. (b) The knock-on D spectrum, with a yield of about 1.7×10^{9} deuterons under the high-energy peak (between 3.5–12 MeV). An energy loss of about 4.1 MeV is measured. (c) The knock-on p spectrum, with a yield of about 2.0×10^{9} MeV protons in the flat region between 8–12 MeV. As in Fig. 5, the endpoint of this spectrum is about 14 MeV, reflecting the fact that particles scattered from the outer part of the shell have no energy loss.

the fact that protons scattered from the outer part of the shell lose no energy. We note that CPS yield measurements represent an integral over the fusion burn duration, so an inferred ρR value represents an average over the burn. In addition, the fact that the source of neutrons is distributed over a finite volume of fuel means that inferred ρR values represent spatial averages.

The measured knock-on spectra for shot 20698 are shown in Fig. 6. The capsule was filled with 15 atm of DT gas and had a 19.9-μm CH shell. The laser energy was 23.8 kJ, and the primary neutron yield was $1.4(\pm0.1)\times10^{13}$. In contrast to shot 20231, polarization smoothing was applied for this shot and the 2D–SSD bandwidth was increased to 1.0 THz. The beam-to-beam energy balance (3.1% rms) and the on-target low-mode rms uniformity (1.3% rms) were thus improved. An ion temperature of $T_i\cong4.1(\pm0.5)$ keV was obtained. The fusion burn occurred at $1750(\pm50)$ ps and lasted for $170(\pm25)$ ps. Figure 6(a) shows the knock-on T spectrum, with a yield of about 1.2×10^{9} tritons under the high-energy peak (between 2.5–10 MeV). [In principle, since the effective cross section for knock-on tritons is larger than that for deuterons (0.1426 vs 0.1046), the triton yield should be higher. However, experimentally, we often measure triton yields equal/less than deuteron yields. A number of reasons could be attributed to this phenomena such as (1) the triton spectrum is usually distorted more due to larger stopping power; and (2) the isotopic composition of the fuel is not exactly equal parts of D and T, although it is difficult, at present, to exactly quantify this effect. And the continuing exchange of both D and T for H does tend to decrease both by a small amount over time. These issues are currently being investigated.] The whole spectrum is downshifted by 4.8 MeV. Figure 6(b) shows the knock-on D spectrum, with a yield of about 1.7×10^{9} deuterons under the high-energy peak (between 3.5–12 MeV). An energy loss of about 4.1 MeV is measured. Figure 6(c) shows the knock-on p spectrum, with a yield of about 2.0×10^{9} MeV in the flat region between 8–12 MeV. The endpoint of this spectrum is about 14 MeV, as it was for shot 20231 (0.35-THz 2D SSD, no PS). Relative to shot 20231, the primary neutron yield in shot 20698 is higher by a factor of $\cong1.95$, and the knock-on particle yields are higher by factors of $\cong3.54$ (deuteron) and $\cong3.51$ (proton). In addition, because of increased compression, the energy loss of the knock-on particles from the fuel is greater by 15–30 %.

V. RESULTS AND DISCUSSIONS

A. Core performance of moderate-convergence capsule implosions

In this section, the measurements of primary neutrons and knock-on charged particles are used to study the effects of illumination uniformity on core performance for moderate-convergence capsule implosions. We start with the primary neutron yield, which provides one direct overall measure of core performance because of its strong dependence upon ion temperature and density. Then we look at the yields of knock-on deuterons ($Y_{\mathrm{KO}d}$) and tritons ($Y_{\mathrm{KO}t}$), which provide a measure of ρR_{fuel}, and thus the amount of compression (which is quantified by the convergence ratio Cr, defined as a ratio of the initial fuel radius to the final compressed fuel radius). After showing that the data demonstrate an improvement of performance with improved laser smoothing, we look at comparisons of the data with numerical simulations. These comparisons suggest that the poorer performance observed with less smoothing is due to intrinsically 2D or 3D effects such as instabilities and mix.

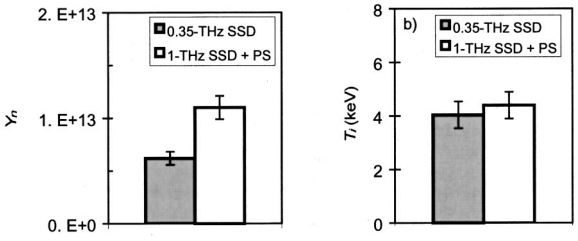

FIG. 7. (a) Average primary yields achieved for two different single-beam smoothing conditions. The yield increases by about 80% when uniformity is improved using 1-THz 2D–SSD+PS. (b) The yield-averaged ion temperature is insensitive to the improvement in uniformity. Consequently, the significant increase of primary yields cannot be attributed to the ion temperatures, and is instead probably a consequence of an increase in ion density due to better fuel compression. The error bars display statistical uncertainties.

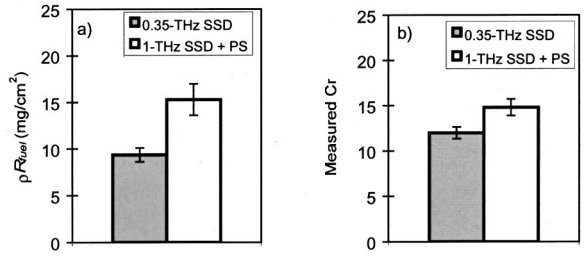

FIG. 8. (a) Average fuel areal densities measured in experiments using 0.35-THz 2D–SSD ($\rho R_{\text{fuel}} \sim 9$ mg/cm^2), and using 1-THz 2D–SSD+PS ($\rho R_{\text{fuel}} \sim 15$ mg/cm^2). A significant increase of the ρR_{fuel} ($\sim$60%) is obtained using 1.0-THz 2D–SSD+PS. (b) Experimentally measured convergence ratios. Cr$\sim$12 for shots using 0.35-THz 2D–SSD, and Cr$\sim$15 for shots using 1-THz 2D–SSD+PS. The error bars display statistical uncertainties.

Primary neutron yields between 3×10^{12} and 1.4×10^{13} were obtained, and in general better energy balance resulted in higher primary neutron yield. The highest yield was obtained for the shot with a low-mode rms nonuniformity of $\sim$1.3% (beam-to-beam energy balance to within 3.1%). Once on-target, low-mode nonuniformity due to beam imbalance has been decreased to the 5% rms range, single-beam nonuniformity becomes more important for determining capsule performance through its effects on high-order mode perturbations. This is illustrated in Fig. 7(a), where we see that beam smoothing with 1-THz 2D–SSD+PS results in a primary yield ($Y_n \sim 1.1\times10^{13}$) about 80% higher than that obtained with 0.35-THz 2D–SSD and no PS ($Y_n \sim 6.2\times10^{12}$). Since the ion temperature is relatively insensitive to rms uniformity improvement, as shown in Fig. 7(b), higher Y_n must result from a higher ion density due to improved fuel compression.

The fuel areal density is determined from knock-on yields. Efforts to match the experimental primary yields by assuming different temperature profiles lead us to prefer the uniform model over the hot-spot model, because highly peaked temperature profiles lead to yields that are too low, so the ρR_{fuel} vs yield relationships shown in Fig. 4 must be modified. The corresponding inferred convergence ratio is $\text{Cr}=\sqrt{\rho R_{\text{fuel}}/\rho R_{\text{fuel0}}}$, where ρR_{fuel0} is the fuel areal density before compression. As shown in Fig. 8, the data lead to average values of $\rho R_{\text{fuel}} \sim 9$ mg/cm^2 (Cr$\sim$12) for the shots using 0.35-THz 2D–SSD, and $\rho R_{\text{fuel}} \sim 15$ mg/cm^2 (Cr$\sim$15) for 1-THz 2D–SSD+PS. Increasing the smoothing rate increased ρR_{fuel} by $\sim$60% and the Cr by $\sim$25%. (In this calculation, we have assumed exactly equal molar quantities of deuterium and tritium.)

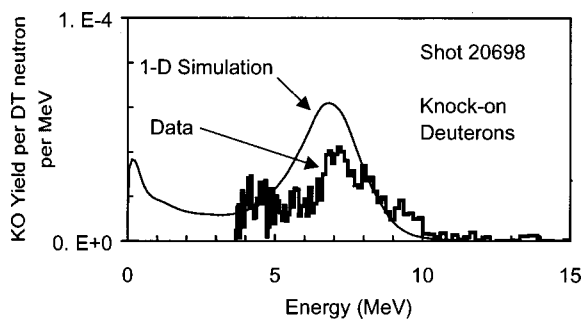

FIG. 9. A comparison of the experimentally measured knock-on deuteron spectrum and the 1D LILAC predicted spectrum for shot 20698.

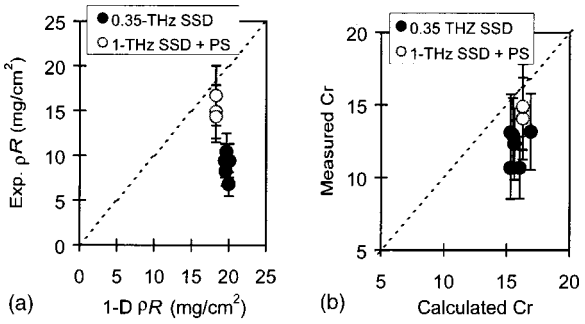

FIG. 10. (a) Measured ρR_{fuel} vs 1D simulation prediction. For the shots with 0.35-THz 2D–SSD, the average measured ρR_{fuel} is about 60% of the prediction. For the shots with 1-THz 2D–SSD+PS, an average of $\sim$80% of the predicted ρR_{fuel} is measured. This comparison suggests that the improvement in irradiation uniformity makes implosions more 1D like. (b) The measured convergence ratio plotted against the calculation. The experimental data are slightly but consistently lower than those of 1D predictions. The error bars display experimental uncertainties ($\sim$10% for neutrons, $\sim$20% for charged particles).

One-dimensional simulations were carried out for these shots, and Fig. 9 shows an example of how a measured knock-on deuteron spectrum compares with a prediction for shot 20698. Relative to the data, the simulation has a similar spectral shape, a similar energy downshift, and a similar, if somewhat higher, yield. Figures 10–13 provide an overview of data-to-simulation comparisons. Since the effects of beam smoothing are intrinsically 2D or 3D, the 1D code predicts no difference due to smoothing, and this can be seen in Figs. 10 and 11, which show that nearly all the shots are predicted to have the same values of ρR_{fuel}, Cr, and T_i, with small differences due only to the small differences in capsule parameters and total laser energy. On the other hand, the measured values of ρR_{fuel} (or Cr) improve significantly for increased laser smoothing, and approach the predicted values with 1-THz 2D–SSD+PS. Other parameters also increase when smoothing is improved, including Y_n and $Y_{\text{KO}d}$, whose ratios to predicted values ("YOC" and $Y_{\text{KO}d}/Y_{\text{1D}}$ respec-

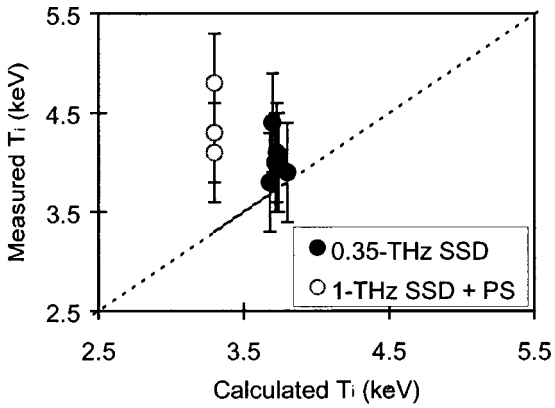

FIG. 11. A comparison of measured ion temperatures to the 1D LILAC predictions, showing that measured values are consistently higher than predictions. The error bars display experimental uncertainty ($\pm$0.5 keV).

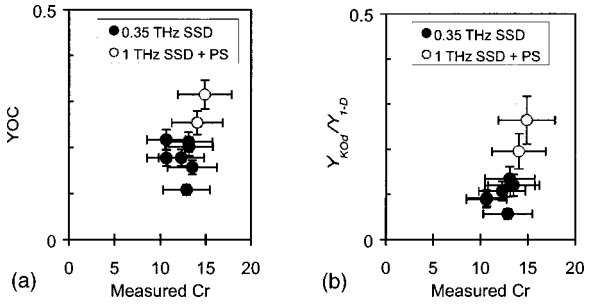

FIG. 12. (a) The ratio of measured primary neutron yield to clean 1D prediction (YOC) plotted against the measured convergence ratio. An average of ~18% is obtained for the shots using 0.35-THz 2D–SSD, while an average of ~30% is obtained for the shots using 1-THz 2D–SSD+PS. (b) The ratio of measured KO deuteron yield to 1D prediction (Y_{KOd}/Y_{1D}) has an average of ~10% for the shots using 0.35-THz 2D–SSD and of ~24% for the shots using 1-THz 2D–SSD+PS. The error bars indicate experimental uncertainties (~10% for neutrons, ~20% for charged particles).

tively) are shown in Fig. 12. Although YOC increases with smoothing, it never exceeds 35% in spite of the fact that T_i and Cr are close to predictions. This could mean, for example, that the burn duration is shorter than predicted, and/or that mix makes the temperature profile more peaked than predicted, reducing the volume of fuel actually participating in the burn. Plotting the ratio of measured to predicted values of Y_{KOd}/Y_n against measured Cr, in Fig. 13, we see that it approaches unity for full beam smoothing. This suggests that the improvement of single-beam irradiation uniformity results in increased compression through the reduction of 2D phenomena such as instabilities and mix.

The credibility of this hypothesis is increased by more elaborate simulations which incorporate effects of RT, Richtmyer–Meshkov, and Bell–Plesset instabilities, and 3D Haan saturation[6,8] in the post-processing of 1D calculation results. It was shown that using 0.35-THz 2D–SSD without PS results in a mix width approaching the in-flight shell thickness.[6,8] The shell integrity is thus reduced, and the capsule compression is degraded. In contrast, the calculations show that with full beam smoothing (on-target beam nonuniformity less than 1% after 300 ps), the mix width is significantly smaller than the in-flight shell thickness.

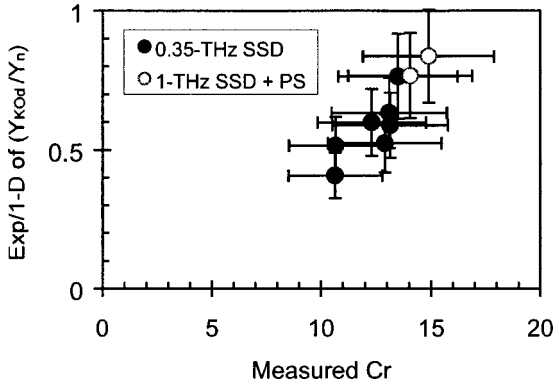

FIG. 13. The ratio of the experimentally measured value of Y_{KOd}/Y_n to the 1D prediction for different measured Cr. About ~60% is obtained for the shots using 0.35-THz. 2D–SSD, and ~80% is obtained for the shots using 1-THz 2D–SSD+PS. This ratio approaches unity, while YOC is considerably smaller (≤30%). The error bars indicate experimental uncertainties (~10% for neutrons, ~20% for charged particles).

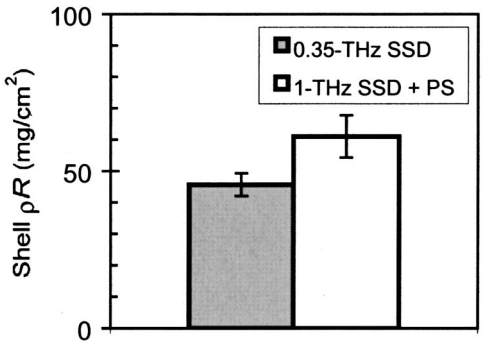

FIG. 14. An average measured ρR_{shell} of ~45 mg/cm^2 is obtained for the shots using 0.35-THz 2D–SSD and ρR_{shell} of ~60 mg/cm^2 is obtained for the shots using 1-THz 2D–SSD+PS. The error bars display statistical uncertainties.

B. Shell performance of moderate-convergence capsule implosions

The shell performance discussed in this section is based on measurements of shell areal density, ρR_{shell}, and shell electron temperature (T_e). ρR_{shell} can be determined directly from the yield of knock-on protons (this is a temperature-independent method). Once ρR_{shell} is known, and ρR_{fuel} has been determined as described in the preceding section, the shell T_e can be estimated from the energy downshift of the deuteron and/or triton spectrum (slowing down of these particles is sensitive to T_e). Alternatively, if the shell T_e is already known from other measurements, then the deuteron and/or triton downshifts can be used in an independent estimation of ρR_{shell}.

Knock-on protons are generated only in the CH shell, and typical proton spectra are shown in Figs. 5(c) and 6(c). Values of ρR_{shell} can be calculated from the proton yields with Fig. 4. As displayed in Fig. 14, an average ρR_{shell} of ~45 mg/cm^2 is obtained for the shots using 0.35 THz 2D–SSD without PS, while an average ρR_{shell} of ~60 mg/cm^2 is obtained for 1 THz 2D–SSD+PS. A 35% increase of the

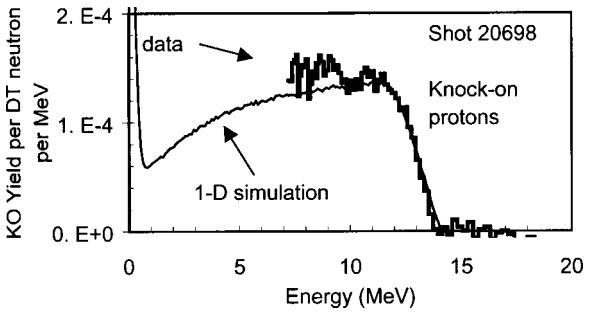

FIG. 15. A comparison of the measured knock-on proton spectrum (thick line) to the 1D LILAC prediction (thin line) for shot 20698. The agreement between these two spectra suggests the compressed shell nearly has 1D performance. (The fact that the predicted spectrum is not flat, and decays in the region between 0–8 MeV, is due to the fact that low-energy protons generated during the stagnation phase of the implosion may experience a large ρR_{shell} and be ranged out.)

ρR_{shell} is thus obtained due to the improvement of single-beam uniformity. Figure 15 displays a 1D calculated knock-on proton spectrum overlaid on an experimentally measured proton spectrum for shot 20698. The agreement between these two spectra suggests that, with full beam smoothing, the shell performance of a moderate-convergence implosion is close to the 1D prediction.

The directly determined value of ρR_{fuel} (described in the preceding section), together with the measured energy loss of the deuteron and/or triton knock-ons, can also be used to determine shell T_e (if ρR_{shell} has been determined as described in the previous paragraph) or to study ρR_{shell} (if the shell T_e is known). As deuteron and/or triton knock-ons from the fuel travel through fuel and shell, they lose an amount of energy directly proportional to the areal density of the materials they pass through (assuming there is no particle acceleration, as discussed in Sec. V E). Because these particles are not so energetic, their stopping power is not characterized as ''cold plasma stopping,'' where there is no temperature dependence, but ''warm plasma stopping,'' where there is a temperature dependence. The energy loss can be calculated from the stopping power in a fully ionized plasma,[35,36]

$$\frac{dE}{dx} = -\left(\frac{Z^2\omega_p e}{v_t}\right)^2 [G(x^{t/f})\ln\Lambda + \theta(x^{t/f})\ln(1.123\sqrt{x^{t/f}})], \tag{7}$$

where $\theta(x^{t/f})$ is a step function and equals 0 (1) when $x^{t/f}<1(>1)$; $\omega_p=(4\pi n_e e^2/m_e)^{1/2}$ is the electron plasma frequency, Z is the charge of the incident charged particle; $v_t(v_f)$ is the velocity of a test (field) charged particle; $x^{t/f}=v_t^2/v_f^2$ and $\ln\Lambda$ is the Coulomb logarithm. $G(x^{t/f})$ is defined as

$$G(x^{t/f}) = \mu(x^{t/f}) - \frac{m_f}{m_t}\left\{\frac{d\mu(x^{t/f})}{dx^{t/f}} - \frac{1}{\ln\Lambda}\left[\mu(x^{t/f}) + \frac{d\mu(x^{t/f})}{dx^{t/f}}\right]\right\}, \tag{8}$$

where $\mu(x^{t/f})=2\int_0^{x^{t/f}} e^{-\xi}\sqrt{\xi}\,d\xi/\sqrt{\pi}$ is the Maxwell integral; and $m_t(m_f)$ is the mass of the test (field) particle. Since the effects of large-angle scattering are negligible for charged particles traveling in plasmas of interest,[36] the areal density that a charged particle travels through with an energy loss $(\Delta E \approx E_0 - E)$ can be approximately determined as

$$\rho R = \int_E^{E_0} \rho\left(\frac{dE}{dx}\right)^{-1} dE. \tag{9}$$

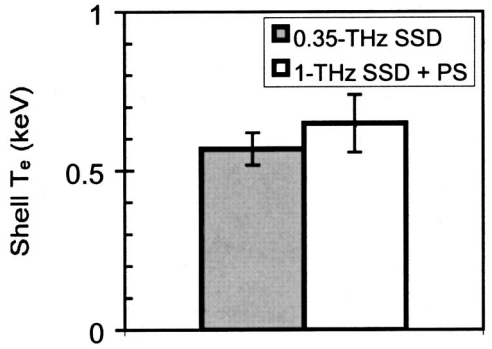

FIG. 16. Average electron temperatures inferred from the knock-on spectra. Values of ~0.58 keV and ~0.65 keV are obtained for the shots using 0.35-THz 2D–SSD and 1-THz 2D–SSD+PS, respectively. The error bars display statistical uncertainties.

Because of the relatively high temperature and low density of the fuel plasma, the energy loss is dominated by the lower temperature but higher density shell plasma. The total areal density is defined as $\rho R_{\text{total}}=\rho R_{\text{fuel}}+\rho R_{\text{shell}}$.

The downshifts of the spectra shown in Figs. 6(a) and 6(b) (for shot 20698) are about 5 MeV for tritons and 4 MeV for deuterons. To be consistent with the temperature-independent, knock-on-derived values of $\rho R_{\text{fuel}}\sim 14\,\text{mg/cm}^2$ and $\rho R_{\text{shell}}\sim 64\,\text{mg/cm}^2$ calculated as described above for this shot, the value of shell T_e must be about 0.6 keV. A summary of calculated shell T_e values for different shots is given in Fig. 16. The shell T_e appears insensitive to single beam irradiation uniformity, to first order, although there are some subtle issues such as time and spatial dependence of the knock-on spectra involved in this determination. This topic will be a subject for future study.

C. Similarity to D_2-filled-capsule implosions

With similar experimental conditions, implosions of DT and D_2 gas-filled plastic capsules are ''hydrodynamically'' equivalent. While some subtle differences, such as the mass, fusion cross-section, equation of the state, etc., still exist, the basic capsule performance is expected to be similar. Recent work[12] has resulted in the study of fuel and shell parameters for D_2 shots at OMEGA by measuring spectra of secondary D ^{3}He protons. Those numbers are very similar to the knock-on-inferred numbers for related DT shots, as shown in Table I. In general, the inferred and estimated ρR_{fuel} and ρR_{shell} and ρR_{total} are very similar for both DT and D_2 capsule implosions under similar experimental conditions. While the

TABLE I. Comparison of DT and D_2 gas-filled, plastic shell implosions (the D_2 numbers are from Ref. 12).

Capsules	Single-beam smoothing	T_i (keV)	Y_n	YOC	$Y_{\text{KO}d}/Y_{1\text{D}}$	$Y_{2p}/Y_{1\text{D}}$	ρR_{fuel} (mg/cm^2)	ρR_{shell} (mg/cm^2)	ρR_{total} (mg/cm^2)
DT(15)CH(20)	0.3 THz 2D–SSD	4.1±0.5	$(6.2\pm1.4)\times10^{12}$	0.18	0.10		9±2	47±7	~56[a]
	1 THz 2D–SSD+PS	4.4±0.5	$(1.1\pm0.3)\times10^{13}$	0.30	0.24		15±3	61±7	~76[a]
D_2(15)CH(20)	0.3 THz 2D–SSD	3.4±0.5	$(8.8\pm0.8)\times10^{10}$	0.18		0.13	10±2	~42[b]	52
	1 THz 2D–SSD+PS	3.7±0.5	$(1.6\pm0.5)\times10^{11}$	0.33		0.21	14+7-4	~58[b]	72

[a]Estimated based on measured ρR_{fuel} and ρR_{shell}.
[b]Estimated based on measured ρR_{fuel} and ρR_{total}.

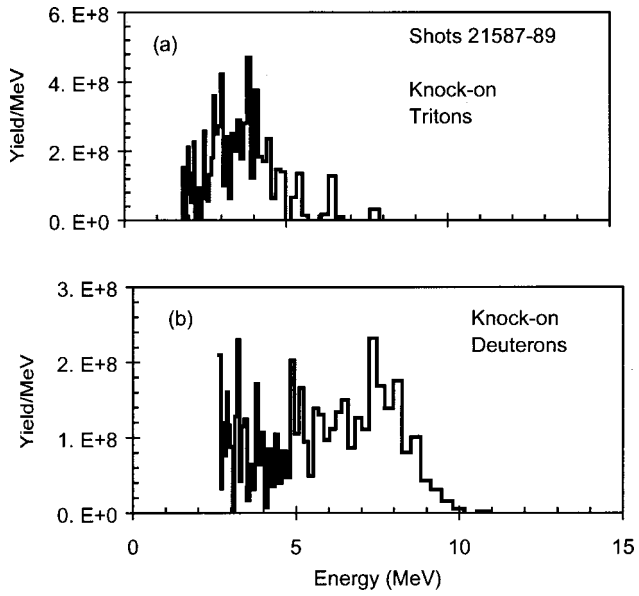

FIG. 17. (a) Knock-on triton spectrum obtained from a 3-shot integration (shots 21587, 21588 and 21589, all implosions of capsules with 3.8-atm DT gas). An average yield of 2×10^8 per shot is obtained, and this implies $\rho R_{\text{fuel}}\sim 3$ mg/cm^2 (assuming a uniform model). (b) Knock-on deuteron spectrum obtained from the same 3-shots. An average yield of 2.1×10^8 per shot is obtained, implying $\rho R_{\text{fuel}}\sim 3$ mg/cm^2 (assuming a uniform model).

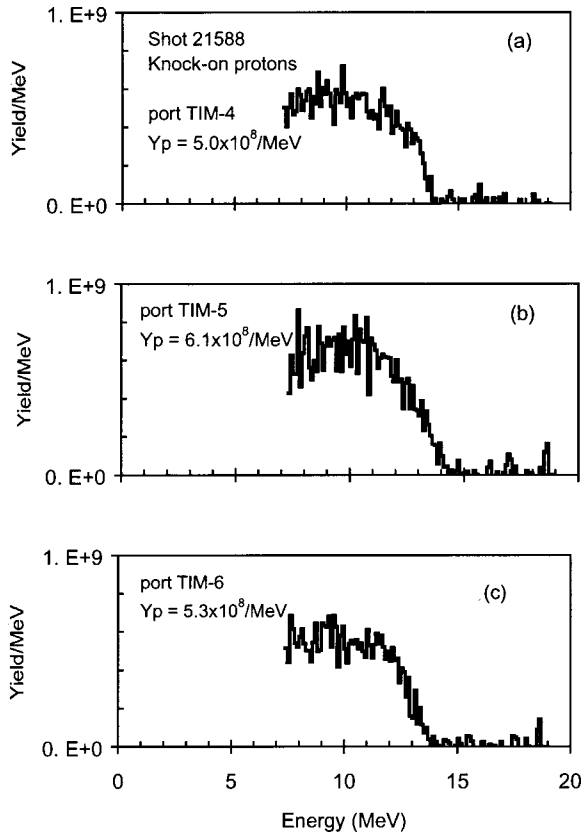

FIG. 18. Knock-on proton spectra of shot 21588, measured using wedge-range-filter spectrometers (WRF) from three different directions. Combined with similar spectra measured for shots 21587 and 21589, we find an average knock-on-proton yield of $\sim 6.2\times10^8$ MeV/shot (in the flat regions of the spectra). This implies an average value of $\rho R_{\text{shell}}\sim 55$ mg/cm^2 for these shots.

corresponding values of YOC are similar, DT implosions result in higher ion temperatures than D_2 implosions. The improvement of the single-beam irradiation uniformity enhances the target performance of both DT and D_2 implosions: $\rho R_{\text{fuel}}(\rho R_{\text{shell}})$ increases by ~60% (~35%) for DT implosions and by ~65% (~40%) for D_2 implosions; Y_n increases by ~80% for both DT and D_2 implosions; YOC increases by ~60% for DT and by ~80% for D_2 implosions. Ion temperatures are not so sensitive to the uniformity improvement ($\leqslant$10%). In summary, implosions of D_2-filled and DT-filled capsules have very similar performance.

D. Preliminary results on "high-convergence" DT-capsule implosions

In order to contrast with the moderate-convergence-ratio (Cr~15) capsule implosions discussed above, we also imploded a small number of DT capsules which were predicted from 1D simulations to have considerably higher convergence (Cr~30; $\rho R_{\text{fuel}}\sim 15$ mg/cm^2; $\rho R_{\text{shell}}\sim 100$ mg/cm^2) under similar experimental conditions (1 THz 2D–SSD with PS). These capsules had ~3.8-atm DT gas fills and CH shells 20 μm thick.

For shots 21587, 21588, and 21589 we obtained an averaged primary neutron yield of $Y_n\sim 4.9\times10^{12}$/shot. The measured knock-on triton and deuteron spectra are shown in Fig. 17, summed over the three shots. The mean triton and deuteron yields were $Y_{\text{KO}t}\sim 2\times10^8$/shot and $Y_{\text{KO}d}\sim 2.1\times10^8$/shot. Figure 18 shows knock-on proton spectra for shot 21588, measured simultaneously from three different directions (using diagnostic ports TIM-4, TIM-5, and TIM-6). A total of eight separate proton spectra were measured for the three shots, with an average knock-on proton yield of $\sim 6.2\times10^8$ MeV/shot.

From these measurements, we infer mean implosion parameters of $\rho R_{\text{fuel}}\sim 3$ mg/cm^2 (uniform model) and $\rho R_{\text{shell}}\sim 55$ mg/cm^2 (hot-spot model). These values are, respectively, about 20% and 55% of the 1D predictions. The corresponding convergence ratios are similar to the values for 15-atm capsules. The performance is degraded relative to 1D prediction and suggests that the effects of mix and instabilities are more deleterious for high convergence implosions. Further detailed studies are planned, and we note that similar implosion parameters have been inferred for implosions of D_2-filled capsules with similar characteristics.[12]

E. Capsule charging and particle acceleration

Time-dependent capsule charging is an essential issue in a spherical implosion. This charging may result in a strong electric field surrounding the capsule and an acceleration of emitted charged particles.[37,38] Since the measurement of areal densities of imploded capsules through charged-particle spectroscopy relies on accurate determination of particle energy downshift due to slowing in the capsule, any particle acceleration could introduce serious errors.

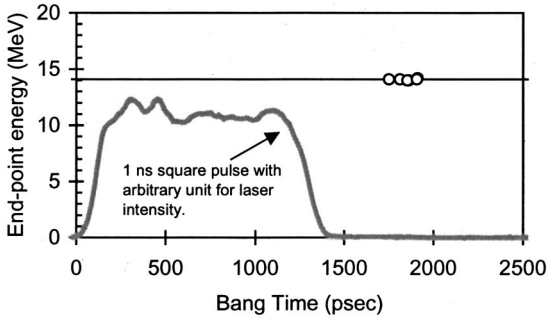

FIG. 19. The measured upper energy endpoints of the knock-on proton spectra of a number of shots in this study are plotted against the bang time (a typical 1-ns square pulse with an arbitrary unit for laser intensity on OMEGA is also displayed for reference). As seen, the laser pulse has completely ended at ~1400 ps, while the bang times occur at 1750–1950 ps. The energies match the maximum scattered-proton energy, indicating that there are no energy up-shifts.

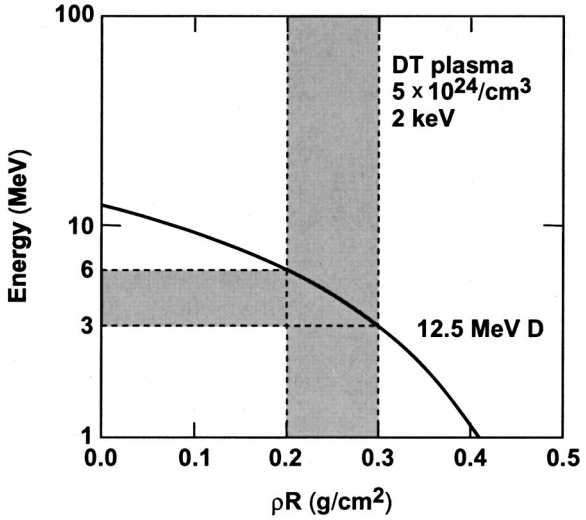

FIG. 20. The energy of knock-on deuterons vs their range (ρR) in a DT plasma. In this calculation, an electron temperature of 2 keV and an ion density of 5×10^{24} have been assumed. For a typical predicted areal density of 200–300 mg/cm^2 for a cryogenic capsule implosion, a knock-on deuteron will lose about 6–9 MeV energy, and the residual energy (3–6 MeV) left after leaving the target is readily detectable using charged-particle spectrometry.

Many previous experiments have demonstrated the existence of capsule charging and particle acceleration, even (unexpectedly) on OMEGA with laser intensities of $\sim10^{15}$ W/cm^2 and wavelength 351 nm (where energy up-shifts of ~1 MeV have been observed for charged-fusion products and for ablator protons[11,37,38]). The hot electrons generated by laser-plasma instabilities in the corona are thought to cause this capsule charging. Earlier experiments also suggest that the charge is time dependent.

For estimating the effects of the electric fields on charged-fusion products, it has been assumed that such effects are only important when the bang time occurs while the laser is on (for example, for a thin-glass-shell capsule driven by 1-ns square pulse).[39,40] Such effects are assumed to be not important when the bang time occurs several hundreds of ps after the laser turns, off, when the electric field has largely decayed away (for example, a thick-plastic-shell capsule driven by a 1-ns square pulse[11,37]). For the latter case, possible energy up-shifts, if any, have been assumed to be completely negligible. Although widely used when determining the spectral downshifts of charged particles,[11,37] these assumptions have never before been directly proven by experiments because the effects of particle acceleration and slowing down are always mixed in an implosion for charged-fusion products.

The knock-on proton data described in this paper finally provide direct proof of this assumption for thick-plastic-shell capsules driven by 1-ns square laser pulses. Any acceleration would cause the upper endpoints of the knock-on proton spectra to be up-shifted relative to the 14-MeV endpoint of the birth spectrum. In Figs. 5(c) and 6(c), the endpoints of the knock-on proton spectra are precisely (within statistical errors) at 14 MeV, which indicates that the protons are subject to no acceleration. Figure 19 shows the measured endpoints of these and other knock-on proton spectra for a number of shots, plotted against the bang time (a typical 1-ns square pulse on OMEGA is also displayed for reference). The laser pulse has completely ended at ~1400 ps, while the bang time occurs several hundreds of ps later. No energy up-shifts are observed.

F. Relevance to OMEGA cryogenic capsule implosions

At OMEGA, plans exist to implode cryogenic DT capsules which typically have low-pressure DT gas fill in the center surrounded by about 90 μm of DT ice with ~2 μm CH as an ablator. These implosions are predicted to generate DT primary yields $>10^{13}$, with ion temperature between 1–4 keV and areal densities up to ~300 mg/cm^2. Nuclear diagnostics will play an important role in the OMEGA cryogenic program. Figure 20 shows the energy of knock-on deuterons plotted against their range (ρR) in a DT plasma (an electron temperature of 2 keV and an ion density of 5×10^{24} are assumed, although the density effects on these calculations are weak[35,36]). For a typical areal density of 200–300 mg/cm^2, a knock-on deuteron will lose about 6–9 MeV as it traverses the capsule, and the remaining energy of 3–6 MeV is readily detectable using CPS.[24]

VI. SUMMARY AND CONCLUSIONS

Direct-drive implosions of DT-gas-filled plastic capsules were studied using nuclear diagnostics on OMEGA. In addition to the traditional neutron measurements, comprehensive and high-resolution spectra of knock-on deuterons, tritons, and protons were obtained for the first time in ICF experiments and used for characterizing target performance.

It was determined that an improvement in target performance is achieved, for moderate-convergence implosions (Cr~10–20), with the reduction of on-target irradiation nonuniformity that results from an improvement of beam-to-beam laser energy balance and from an enhancement of single-beam uniformity. With the use of a 1-THz bandwidth of smoothing by spectral dispersion and polarization smoothing, $Y_n\sim1.1\times10^{13}$, YOC~0.3, $\rho R_{\text{fuel}}\sim15$ mg/cm^2, and $\rho R_{\text{shell}}\sim60$ mg/cm^2, which are, respectively, approximately

80%, 60%, 60%, and 35% higher than those determined when using a 0.35 THz bandwidth of smoothing by spectral dispersion. Polarization smoothing of individual laser beams is believed to play an important role.

With full beam smoothing, these implosions have some performance parameters close to one-dimensional-code predictions (e.g., measured ratio of $Y_{\mathrm{KO}d}/Y_n$ achieve ~80% of 1D predictions). Data suggest that high irradiation uniformity results in reduced Rayleigh–Taylor growth and improved shell integrity. For the same smoothing conditions, however, capsules that should reach high convergence (3.8-atm DT gas fill, 20-μm CH shell, and predicted Cr~30) showed substantially degraded performance relative to 1D predictions (measured $\rho R_{\mathrm{fuel}} \sim 3$ mg/cm^2 and measured convergence ratios similar to the values for 15-atm capsules). This indicates that the effects of mix are, not surprisingly, more deleterious for high-convergence implosions. In addition, a brief comparison demonstrates the hydrodynamic ''equivalence'' of DT-filled capsules and D_2-filled capsules for both moderate- and high-convergence implosions.

ACKNOWLEDGMENTS

We express our appreciation to the OMEGA Laser and Experimental Operation and Target Fabrication crews for their excellent work and continuous support. This work has been supported in part by LLE (subcontract P0410025G) and LLNL (subcontract B313975), and by the U.S. Department of Energy Office of Inertial Confinement Fusion under Cooperative Agreement No. DE-FC03-92SF19460, the University of Rochester, and New York State Energy Research and Development Authority. The support of DOE does not constitute an endorsement by DOE of the views expressed in this work.

[1] J. D. Lindl, R. L. McCrory, and E. M. Campbell, Phys. Today **45**, 32 (1992).
[2] J. D. Lindl, *Intertial Confinement Fusion* (Springer-Verlag, New York, 1999).
[3] S. W. Haan, S. M. Pollaine, J. D. Lindl *et al.*, Phys. Plasmas **2**, 2480 (1995).
[4] P. W. McKenty, V. N. Gonchahrov, R. P. J. Town, R. Betti, and S. Skupsky, Phys. Plasmas **8**, 2315 (2001).
[5] T. R. Boehly, D. L. Brown, R. S. Craxton *et al.*, Opt. Commun. **133**, 495 (1997).
[6] R. L. McCrory, R. E. Bahr, R. Betti *et al.*, OMEGA ICF experiments and preparation for direct-drive ignition on NIF, *Proceedings of the 18th IAEA Fusion Energy Conference* (International Atomic Energy Agency, Vienna, in press).
[7] J. M. Soures, R. L. McCrory, C. P. Verdon *et al.*, Phys. Plasmas **3**, 2108 (1996).
[8] D. D. Meyerhofer, J. Delettrez, R. Epstein *et al.*, Phys. Plasmas **8**, 2251 (2001).
[9] F. J. Marshall, J. Delettrez, V. Yu. Glebov, R. P. J. Town, B. Yaakobi, R. L. Kremens, and M. D. Cable, Phys. Plasmas **7**, 1006 (2000).
[10] F. J. Marshall, J. Delettrez, R. Epstein *et al.*, Phys. Plasmas **7**, 2108 (2000).
[11] C. K. Li, D. G. Hicks, F. H. Séguin *et al.*, Phys. Plasmas **7**, 2578 (2000).
[12] F. H. Séguin, C. K. Li, J. A. Frenje *et al.*, ''Using secondary proton spectra to study imploded D_2-filled capsules at OMEGA laser facility,'' submitted to Phys. Plasmas.
[13] F. H. Séguin (private communication).
[14] P. B. Radha, S. Skupsky, R. D. Petrasso, and J. M. Soures, Phys. Plasmas **7**, 1531 (2000).
[15] S. Skupsky and R. S. Craxton, Phys. Plasmas **6**, 2157 (1999).
[16] V. Yu. Glebov, D. D. Meyerhofer, and C. Stoeckl, Bull. Am. Phys. Soc. **45**, 145 (2000).
[17] M. A. Russotto and R. L. Kremens, Rev. Sci. Instrum. **61**, 3125 (1990).
[18] J. D. Kilkenny, M. D. Cable, C. A. Clower *et al.*, Rev. Sci. Instrum. **66**, 288 (1995).
[19] R. J. Leeper, G. A. Chandler, G. W. Cooper *et al.*, Rev. Sci. Instrum. **68**, 868 (1997).
[20] R. A. Lerche, D. W. Phillion, and G. L. Tietbohl, Rev. Sci. Instrum. **66**, 933 (1995).
[21] R. J. Leeper, J. R. Lee, L. Kissel, D. J. Johnson, W. A. Stygar, and D. E. Hebron, J. Appl. Phys. **60**, 4059 (1986).
[22] W. A. Stygar, R. J. Leeper, L. P. Mix, E. R. Brock, J. E. Bailey, D. E. Hebron, D. J. Johnson, J. Maenchen, T. A. Mehlhorn, and P. Reyes, Rev. Sci. Instrum. **59**, 1703 (1988).
[23] D. G. Hicks, C. K. Li, D. P. Petrasso, F. H. Seguin, B. E. Burke, J. P. Knauer, S. Cremer, and L. Kremens, Rev. Sci. Instrum. **68**, 589 (1997).
[24] D. G. Hicks, Ph.D. thesis, Massachusetts Institute of Technology, 1999.
[25] S. Skupsky and S. Kacenjar, J. Appl. Phys. **52**, 2608 (1981).
[26] S. Kacenjar, S. Skupsky, A. Entenberg, L. Goldman, and M. Richardson, Phys. Rev. Lett. **49**, 463 (1982).
[27] E. M. Campbell, S. M. Lane, Y. L. Pan, J. T. Larsen, R. J. Wahl, and R. H. Price, J. Appl. Phys. **51**, 6062 (1980).
[28] M. D. Cable and S. P. Hatchett, J. Appl. Phys. **62**, 2233 (1987).
[29] H. Azechi, M. D. Cable, and R. O. Stapf, Laser Part. Beams **9**, 119 (1991).
[30] R. D. Petrasso, C. K. Li, M. D. Cable *et al.*, Phys. Rev. Lett. **77**, 2718 (1996).
[31] S. Cremer, C. P. Verdon, and R. D. Petrasso, Phys. Plasmas **5**, 4009 (1998).
[32] J. P. Knauer, R. L. Kremens, M. A. Russotto, and S. Tudman, Rev. Sci. Instrum. **66**, 926 (1995).
[33] M. D. Cable, S. P. Hatchett, and M. B. Nelson, Rev. Sci. Instrum. **63**, 4823 (1992).
[34] E. B. Goldman, Laboratory for Laser Energetics Report No. 16, University of Rochester, 1973.
[35] C. K. Li and R. D. Petrasso, Phys. Rev. Lett. **70**, 3059 (1993).
[36] C. K. Li and R. D. Petrasso, Phys. Plasmas **2**, 2460 (1995).
[37] D. G. Hicks, C. K. Li, F. H. Séguin *et al.*, Phys. Plasmas **7**, 5106 (2000).
[38] D. G. Hicks, C. K. Li, F. H. Séguin *et al.*, Phys. Plasmas **8**, 606 (2001).
[39] Y. Gazit, J. Delettrez, T. C. Bristow, A. Entenberg, and J. M. Soures, Phys. Rev. Lett. **43**, 1943 (1979).
[40] J. Delettrez, A. Entenberg, Y. Gzit, D. Shvarts, J. Virmont, T. Bristow, J. M. Soures, and A. Bennish, Nucl. Fusion **23**, 1135 (1983).